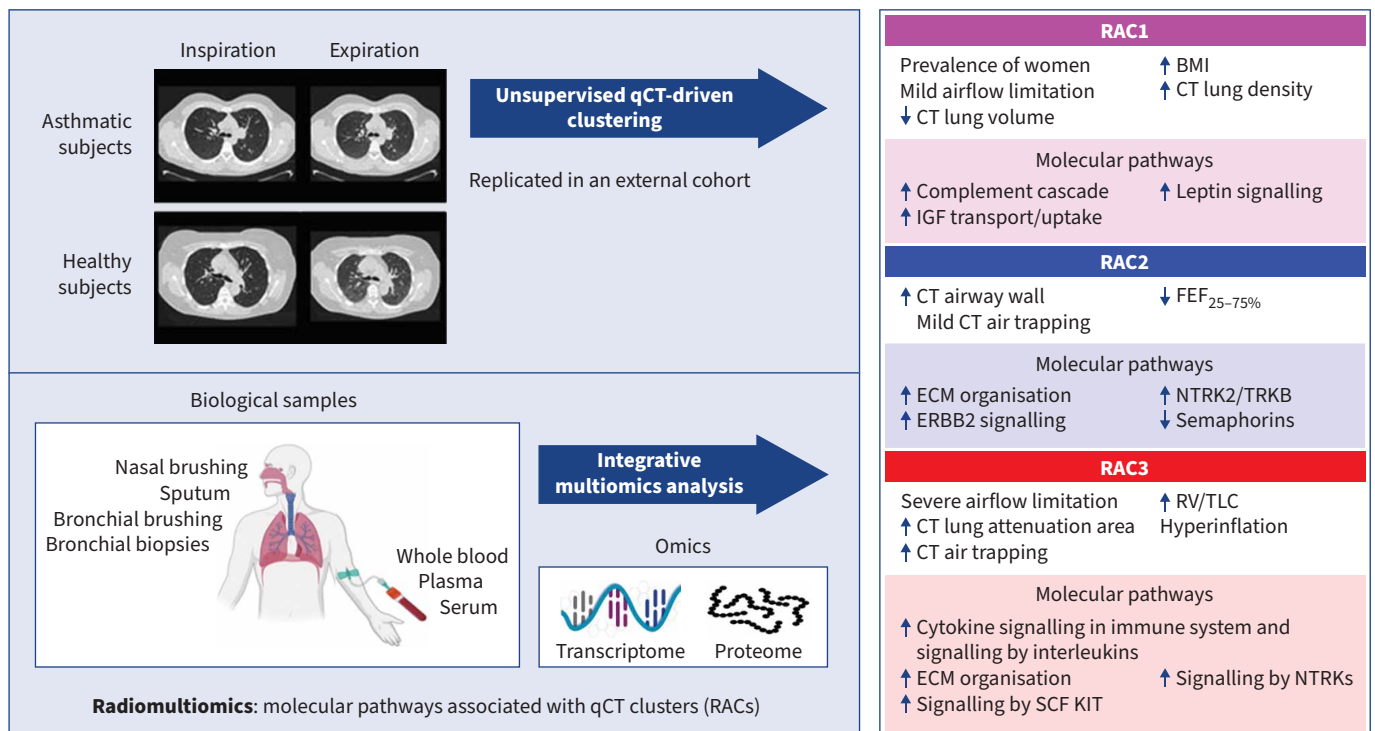




Radiomultiomics: quantitative CT clusters of severe asthma associated with multiomics

Nazanin Zounemat Kermani, Kian Fan Chung, Giuseppe Macis, Giuseppe Santini, Franz A.A. Clemeno, Ali Versi, Kai Sun, Mahmoud I. Abdel-Aziz , Lars I. Andersson , Charles Auffray, Yusef Badi, Per Bakke, Chris Brightling, Paul Brinkman , Massimo Caruso , Pascal Chanez , Bertrand De Meulder , Ratko Djukanovic, Leonardo Fabbri , Stephen J. Fowler , Ildiko Horvath, Peter Howarth , Anna J. James, Johan Kolmert , Monica Kraft, Chuan-Xing Li, Anke H. Maitland-van der Zee, Mario Malerba, Alberto Papi, Klaus Rabe, Marek Sanak, Dominick E. Shaw , Dave Singh, Maria Sparreman Mikus , Maarten van Den Berge, Asa M. Wheelock, Craig E. Wheelock , Valentyna Yasinska , Yi-ke Guo, Scott Wagers, Peter J. Barnes, Andrew Bush , Peter J. Sterk, Sven-Erik Dahlen, Ian M. Adcock , Salman Siddiqui and Paolo Montuschi on behalf of the U-BIOPRED and ATLANTIS Study Groups



GRAPHICAL ABSTRACT Overview of the study. (q)CT: (quantitative) computed tomography; RAC: radiomultiomic-associated cluster; BMI: body mass index; IGF: insulin-like growth factor; FEF_{25-75%}: forced expiratory flow at 25–75% of forced vital capacity; ECM: extracellular matrix; RV: residual volume; TLC: total lung capacity. See the supplementary material for a full list of definitions of abbreviations of genes, proteins and pathways.



Radiomultiomics: quantitative CT clusters of severe asthma associated with multiomics

Nazanin Zounemat Kermani¹, Kian Fan Chung^{2,3}, Giuseppe Macis⁴, Giuseppe Santini⁵, Franz A.A. Clemeno⁶, Ali Versi¹, Kai Sun¹, Mahmoud I. Abdel-Aziz⁷, Lars I. Andersson^{8,9}, Charles Auffray¹⁰, Yusef Badi¹, Per Bakke¹¹, Chris Brightling¹², Paul Brinkman⁷, Massimo Caruso¹³, Pascal Chanez¹⁴, Bertrand De Meulder¹⁰, Ratko Djukanovic¹⁵, Leonardo Fabbri¹⁶, Stephen J. Fowler¹⁷, Ildiko Horvath¹⁸, Peter Howarth¹⁵, Anna J. James¹⁹, Johan Kolmert²⁰, Monica Kraft²¹, Chuan-Xing Li²², Anke H. Maitland-van der Zee⁷, Mario Malerba²³, Alberto Papi¹⁷, Klaus Rabe²⁴, Marek Sanak²⁵, Dominick E. Shaw²⁶, Dave Singh²⁷, Maria Sparreman Mikus⁸, Maarten van Den Berge²⁸, Asa M. Wheelock²², Craig E. Wheelock²⁰, Valentyna Yasinska^{8,9}, Yi-ke Guo¹, Scott Wagers²⁹, Peter J. Barnes², Andrew Bush², Peter J. Sterk⁷, Sven-Erik Dahlen^{8,9,20}, Ian M. Adcock^{2,30}, Salman Siddiqui^{2,30} and Paolo Montuschi^{2,5,30} on behalf of the U-BIOPRED and ATLANTIS Study Groups

¹Data Science Institute, Imperial College London, London, UK. ²National Heart and Lung Institute, Imperial College London, London, UK. ³Royal Brompton and Harefield Hospitals, London, UK. ⁴Radiology, Faculty of Medicine, Catholic University of the Sacred Heart, Rome, Italy. ⁵Pharmacology, Faculty of Medicine, Catholic University of the Sacred Heart, Rome, Italy. ⁶Department of Respiratory Sciences, University of Leicester, Leicester, UK. ⁷Department of Pulmonology, Amsterdam UMC, University of Amsterdam, Amsterdam, The Netherlands. ⁸Department of Medicine Huddinge, Karolinska Institutet, Stockholm, Sweden. ⁹Department of Respiratory Medicine, Karolinska University Hospital, Stockholm, Sweden. ¹⁰European Institute for Systems Biology and Medicine, CNRS-ENS-UCBL-INSERM, Université de Lyon, Lyon, France. ¹¹Department of Clinical Science, University of Bergen, Bergen, Norway. ¹²Institute for Lung Health, NIHR Leicester Biomedical Research Centre, Department of Respiratory Sciences, University of Leicester, Leicester, UK. ¹³Department of Biomedical and Biotechnological Sciences, University of Catania, Catania, Italy. ¹⁴AP-HM – Clinique des Bronches, Allergies et Sommeil, Aix Marseille Université, Marseille, France. ¹⁵NIHR Southampton Respiratory Biomedical Research Unit and Clinical and Experimental Sciences, University of Southampton, Southampton, UK. ¹⁶Respiratory Medicine, Department of Translational Medicine, University of Ferrara, Ferrara, Italy. ¹⁷Division of Infection, Immunity and Respiratory Medicine, School of Biological Sciences, University of Manchester, Manchester University NHS Foundation Trust, Manchester Academic Health Science Centre, Manchester, UK. ¹⁸Semmelweis University, Budapest, Hungary. ¹⁹Department of Women's and Children's Health, Karolinska Institutet, Stockholm, Sweden. ²⁰Institute of Environmental Medicine, Centre for Allergy Research, Karolinska Institutet, Stockholm, Sweden. ²¹Samuel Bronfman Department of Medicine, Icahn School of Medicine at Mount Sinai Hospital, New York, NY, USA. ²²Department of Medicine Solna, Karolinska Institutet, Stockholm, Sweden. ²³Department of Translational Medicine, University of Piemonte Orientale, Novara, Italy. ²⁴LungenClinic Grosshansdorf and Department of Medicine, Christian Albrechts University, Airway Research Center North within the German Center for Lung Research (DZL), Kiel, Germany. ²⁵Division of Clinical Genetics and Molecular Biology, Department of Medicine, Jagiellonian University Medical College, Kraków, Poland. ²⁶Respiratory Research Unit, University of Nottingham, Nottingham, UK. ²⁷Centre for Respiratory Medicine and Allergy, Manchester University NHS Foundation Hospital Trust, University of Manchester, Manchester, UK. ²⁸Department of Pulmonology, University of Groningen, University Medical Center Groningen, Groningen, The Netherlands. ²⁹Biosci Consulting, Maasmechelen, Belgium. ³⁰I.M. Adcock, S. Siddiqui and P. Montuschi contributed equally to this article as lead authors and supervised the work.

Corresponding author: Paolo Montuschi (paolo.montuschi@unicatt.it; p.montuschi@imperial.ac.uk)



Shareable abstract (@ERSpublications)

Severe asthma qCT clusters are replicable and associated with selective molecular pathways. By clarifying the potential pathogenetic mechanisms underlying its heterogeneity, radiomultiomics might improve severe asthma personalised medicine. <https://bit.ly/3WfySPI>

Cite this article as: Zounemat Kermani N, Chung KF, Macis G, *et al.* Radiomultiomics: quantitative CT clusters of severe asthma associated with multiomics. *Eur Respir J* 2024; 64: 2400207 [DOI: 10.1183/13993003.00207-2024].

Copyright ©The authors 2024.

Abstract

Background Lung quantitative computed tomography (qCT) severe asthma clusters have been reported, but their replication and underlying disease mechanisms are unknown. We identified and replicated qCT clusters of severe asthma in two independent asthma cohorts and determined their association with molecular pathways, using radiomultiomics, integrating qCT, multiomics and machine learning/artificial intelligence.

This version is distributed under the terms of the Creative Commons Attribution Licence 4.0.

This article has an editorial commentary:
<https://doi.org/10.1183/13993003.01639-2024>

Received: 1 Feb 2024
Accepted: 21 July 2024



Methods We used consensus clustering on qCT measurements of airway and lung CT scans, performed in 105 severe asthmatic adults from the U-BIOPRED cohort. The same qCT measurements were used to replicate qCT clusters in a subsample of the ATLANTIS asthma cohort (n=97). We performed integrated enrichment analysis using blood, sputum, bronchial biopsies, bronchial brushings and nasal brushings transcriptomics and blood and sputum proteomics to characterise radiomultiomic-associated clusters (RACs).

Results qCT clusters and clinical features in U-BIOPRED were replicated in the matched ATLANTIS cohort. In the U-BIOPRED cohort, RAC1 (n=30) was predominantly female with elevated body mass index, mild airflow limitation, decreased CT lung volume and increased lung density and upregulation of the complement pathway. RAC2 (n=34) subjects had airway wall thickness and a mild degree of airflow limitation, with upregulation of proliferative pathways including neurotrophic receptor tyrosine kinase 2/tyrosine kinase receptor B, and downregulation of semaphorin pathways. RAC3 (n=41) showed increased lung attenuation area and air trapping, severe airflow limitation, hyperinflation, and upregulation of cytokine signalling and signalling by interleukin pathways, and matrix metalloproteinase 1, 2 and 9.

Conclusions U-BIOPRED severe asthma qCT clusters were replicated in a matched independent asthmatic cohort and associated with specific molecular pathways. Radiomultiomics might represent a novel strategy to identify new molecular pathways in asthma pathobiology.

Introduction

In asthma, quantitative high-resolution computed tomography (HRCT) (qCT) has revealed that bronchial wall thickening and/or air trapping is related to airflow obstruction, bronchodilator response [1, 2], asthma severity [3–5] and neutrophilic inflammation [6]. In addition, qCT identifies phenotypes of asthma derived from cluster analysis of clinical features [2, 7]. Furthermore, qCT phenotypes themselves are also characterised by varying degrees of luminal and airway wall changes and of air trapping reflecting asthma severity and degrees of airflow obstruction [8–10].

Here, we used qCT measurements from lung HRCT scans of the U-BIOPRED (Unbiased BIOMarker in Prediction of REspiratory Disease outcomes) asthma cohort [11] to identify qCT clusters and externally replicate them in the matched ATLANTIS (AssessmenT of smalL Airways involvemeNT In aSthma) cohort [12]. We further hypothesised that the clusters' association to omics data from different airway compartments and blood would reveal pathways that are potentially associated with qCT clusters (radiomultiomic-associated clusters (RACs)). We refer to this approach as integrated radiomultiomics, based on a combination of qCT, transcriptomics and proteomics, and machine learning/artificial intelligence (AI). In an exploratory study, we linked these qCT clusters to molecular pathways derived from a transcriptomic and proteomic analysis obtained in patients from the U-BIOPRED study.

Methods

Participants

This proof-of-concept study used cross-sectional data from the multicentre pan-European U-BIOPRED study, including a baseline visit and a longitudinal visit 12–18 months apart [11]. The U-BIOPRED adult cohort (ClinicalTrials.gov: NCT01976767) included severe asthma non-smokers (n=311), severe asthma current or ex-smokers (>5 pack-years) (n=110), mild-to-moderate asthma subjects (n=88) and healthy control non-smoking participants (n=101) [11]. The flowchart of the study population selection process is shown in supplementary figure S1. Classification of asthma severity was based on international guidelines [13]. Severe and mild-to-moderate asthma participants were on maintenance treatment with inhaled corticosteroids quantified as fluticasone propionate equivalent at a daily dose of ≥ 500 and $< 500 \mu\text{g}\cdot\text{day}^{-1}$, respectively [11]. All participant data were stored in the TranSMART data management system [14]. The U-BIOPRED study was approved by the ethics committee at each recruiting centre. Written informed consent was obtained from all participants.

Quantitative HRCT

Lung HRCT was performed in 105 asthma participants in the U-BIOPRED study: 73 severe asthma non-smokers, 20 severe asthma current/ex-smokers, 12 mild-to-moderate asthma subjects and 15 healthy control participants (supplementary table S1). Volumetric whole-lung CT scans were obtained at total lung capacity (TLC) and residual volume (RV) following a standardised protocol [15]. Apollo software (VIDA Diagnostics, Coralville, IA, USA) was used for qCT [15]. Parameters reflecting 1) airway morphometry, including lumen area (LA), wall area (WA) and wall area as a percentage of total area (Pct WA), 2) emphysematous-like changes, including inspiratory percentage of low attenuation area with CT number frequency distribution < -950 HU (LAA -950 HU), mean lung density standard deviation of CT numbers (MLD SD) and the 15th percentile of the cumulative frequency distribution of CT numbers (percentile 15),

and 3) air trapping, including expiratory percentage of low attenuation area with CT numbers < -856 HU (LAA -856 HU) were measured (supplementary table S2).

Replication of qCT clusters

We performed internal replication of qCT clusters by splitting the U-BIOPRED dataset ($n=105$) into a training set (70% of the samples), which was used to build the model, and a testing set (30% of the samples), which was used for testing the model. Our external replication plan of the U-BIOPRED qCT clusters involved: 1) measuring compatibility between U-BIOPRED and ATLANTIS [12] demographic, physical–clinical and qCT variables, 2) matching cohorts for asthma severity and demographic characteristics, 3) using the same qCT measurements and machine learning workflow in both cohorts, and 4) examining whether U-BIOPRED and ATLANTIS qCT clusters were similar. More detailed methodology and a description of the analysis is provided in the supplementary material.

ATLANTIS is a multinational prospective asthma cohort of approximately 1000 individuals across nine countries (ClinicalTrials.gov: NCT01976767) [12]. We used the MatchIt R function [16] to identify an ATLANTIS subpopulation that matched U-BIOPRED. Individuals from the external replication cohort were selected to match patients in the U-BIOPRED cohort based on clinical and demographic features, including asthma severity. Individuals were not selected based on CT scan parameters. Therefore, ATLANTIS qCT clusters were used to replicate U-BIOPRED qCT clusters in similar populations. Although we could replicate qCT clusters, we could not replicate RACs as no corresponding omics datasets are available.

Integration of qCT data and clustering

All analyses were performed in R version 4.1.2 (www.r-project.org) and Cytoscape 3.9.1 [17]. 50 qCT parameters were analysed (supplementary table S2). When two or more parameters were highly correlated (absolute Spearman $\rho \geq 0.85$), the most significant was selected.

Consensus clustering (R package ConsensusClusterPlus), applied to individuals with asthma only, was used to find the optimal number of RACs [18], using combined inspiratory and expiratory qCT data.

Integrated functional analysis

We performed an integrated enrichment analysis to identify molecular phenotypes using transcriptomics (blood, sputum, bronchial brushings/bronchial biopsies and nasal brushings) and proteomics (plasma Human Protein Atlas antibody bead array, serum and sputum somaSCAN, and sputum LC-MSMS) datasets from U-BIOPRED [14]. First, we performed differential gene and protein expression analysis across and between the RACs (supplementary tables S3–S5).

p-values were used to prioritise genes/proteins by ActivePathways, utilising p-value merging to combine signals at the gene or protein level (evidence), followed by ranked hypergeometric tests to identify enriched pathways and processes [19]. p-values were merged row-wise using the Brown one-sided method [20] to obtain a single p-value for each gene across the various omics datasets. Pathway over-representation analysis was then conducted on the integrated gene list. Finally, by comparing gene lists of the identified pathways with the differentially expressed genes (DEGs) identified from each omics dataset, we determined the intersection between the pathway genes and the DEGs, providing supporting evidence for the identified pathways per omics dataset. p-values were adjusted by Benjamini–Hochberg false discovery rate. For each comparison and all omics, ActivePathways was run once with Reactome database version 84 [21].

We used Cytoscape [17] and the ActivePathways results are represented as enrichment maps, with nodes corresponding to pathways. Pathways with many shared genes are connected into networks. To further understand the overall expression of genes/proteins of the over-represented pathways across RACs, we created gene/protein signatures using the overlapped genes/proteins between omics data and pathways.

For each signature, we calculated the enrichment scores of the signature in the relevant omics datasets using gene set variation analysis (R package GSVA) [22]. We used the Kruskal–Wallis test for multiple comparisons and the Mann–Whitney U-test for pairwise comparisons of enrichment scores between any two RACs.

Results

Consensus clustering

Three RACs, RAC1 consisting of 30, RAC2 consisting of 34 and RAC3 consisting of 41 asthma participants (table 1 and supplementary table S6), were identified from consensus clustering (supplementary

TABLE 1 Representative characteristics of radiomultiomic-associated clusters (RACs)

	RAC1		RAC2		RAC3		p-value	RAC1 versus RAC2 p-value	RAC1 versus RAC3 p-value	RAC2 versus RAC3 p-value
	n	n	n	n	n	n				
Participants, n	30	34	34	41						
Female, %	77 (n=23)	30	56 (n=19)	34	41 (n=17)	41	0.0128	0.1145	0.0039	0.2508
Age, years	48.4±2.6	30	49.9±2.9	34	52.4±1.7	41	0.6033	0.6778	0.1870	0.3874
BMI, kg·m ⁻²	36.8±1.4	30	27.9±0.8	34	27.8±0.8	41	<0.0001	<0.0001	<0.0001	0.9455
Mild-to-moderate asthma subjects, n	1	30	7	34	4	41	0.0874	0.0575	0.3881	0.2092
Asthma exacerbations in previous 12 months, n	2.5 (1.0–4.0)	30	2.0 (0–4.0)	34	1.0 (0–3.0)	41	0.0851	0.1997	0.0237	0.9180
Pre-bronchodilator FEV ₁ , % pred	70.6 (59.6–90.1)	30	86.5 (71.9–98.1)	34	50.5 (38.5–78.2)	40	<0.0001	0.0393	0.0106	<0.0001
Pre-bronchodilator FVC, % pred	86.0±3.8	30	99.8±2.8	34	84.5±3.2	40	0.0017	0.0042	0.7561	0.0006
Pre-bronchodilator FEV ₁ /FVC, %	70.8±2.6	30	70.4±1.5	34	53.9±1.9	40	<0.0001	0.8769	<0.0001	<0.0001
Pre-bronchodilator FEF _{25–75%} , L·s ⁻¹	1.3 (0.8–2.1)	30	1.7 (0.9–2.5)	34	0.7 (0.4–1.0)	40	0.0001	0.2705	0.0093	<0.001
Pre-bronchodilator FEF _{25–75%} , % pred	37.6 (22.7–57.9)	30	46.0 (27.5–65.5)	34	19.1 (13.1–37.8)	40	<0.0001	0.3366	0.0069	<0.0001
Pre-bronchodilator PEF, % pred	82.1 (64.4–92.2)	30	87.7 (74.3–103.3)	32	58.9 (42.0–80.1)	38	<0.0001	0.0974	0.0087	<0.0001
Change in FEV ₁ , post-salbutamol, %	12.6 (3.0–29.8)	30	10.3 (4.2–13.8)	34	19.1 (6.6–27.1)	40	0.0181	0.2356	0.3138	0.0022
RV, L	2.0 (1.4–2.6)	23	2.1 (1.5–2.5)	26	2.8 (2.5–3.5)	34	<0.0001	0.6230	0.0002	<0.0001
TLC, L	5.0 (4.7–5.6)	23	6.0 (5.0–7.0)	26	7.3 (5.9–7.9)	34	<0.0001	0.0019	<0.0001	0.0040
RV/TLC	0.39±0.03	23	0.35±0.02	26	0.44±0.02	34	0.0191	0.2775	0.1412	0.0035
sG _{aw} , kPa ⁻¹ ·s ⁻¹	0.6 (0.2–1.8)	21	1.1 (0.7–1.8)	23	0.6 (0.3–0.8)	34	0.0104	0.1654	0.3284	0.0012
ACQ-5, average score	2.4±0.2	29	1.7±0.2	30	2.3±0.2	37	0.0604	0.0195	0.6292	0.0669
Current/ex-smokers/non-smokers, n	0/9/21	30	2/7/25	34	5/11/25	41	0.2913	0.3077	0.1396	0.4643
Pack-years, n	10.0 (1.7–15.3)	9	5.2 (4.0–23.0)	9	10.0 (3.0–22.5)	15	0.7241	0.4885	0.5483	0.8264
F _{ENO} , ppb	26.0 (14.5–79.5)	25	32.3 (18.1–50.4)	34	30.0 (19.0–59.0)	39	0.9756	0.9787	0.8350	0.8755
Blood eosinophils, cells·μL ⁻¹	180 (100–300)	29	200 (100–500)	33	300 (180–500)	41	0.0781	0.1308	0.0313	0.3738
Blood neutrophils, cells·μL ⁻¹	4700 (3600–7050)	29	4200 (3050–6445)	33	4690 (3295–7600)	41	0.5306	0.2419	0.5396	0.6323
Sputum eosinophils counts, % [#]	4.4 (0.7–20.0)	12	2.1 (0.8–9.5)	18	6.0 (0.4–32.9)	20	0.8398	0.7230	0.9009	0.5775
Sputum neutrophil counts, % [#]	44.9±4.8	12	53.6±5.6	18	58.0±6.4	20	0.3506	0.2811	0.1626	0.6090

Data for continuous variables are presented as mean±SEM or median (interquartile range); categorical variables are expressed as numbers or percentages. BMI: body mass index; FEV₁: forced expiratory volume in 1 s; FVC: forced vital capacity; FEF_{25–75%}: forced expiratory flow at 25–75% of FVC; PEF: peak expiratory flow; RV: residual volume; TLC: total lung capacity; sG_{aw}: specific airway conductance; ACQ: Asthma Control Questionnaire; F_{ENO}: fractional exhaled nitric oxide. [#]: sputum cell counts are expressed as a percentage of non-squamous cells. Normality of variables was tested using the D'Agostino–Pearson omnibus normality test. Between-group comparisons were performed using ANOVA with Tukey's multiple comparison test for normally distributed data or the Kruskal–Wallis test with Dunn's multiple comparison test for non-parametric data. A Chi-squared test was used for multiple comparisons of categorical variables. If the Chi-squared test was positive, Fisher's exact test was used for pairwise comparisons of categorical variables. Bold indicates significant p-values (p<0.05).

figure S2) of the selected 12 inspiratory and 10 expiratory lung HRCT parameters (supplementary table S7). Consensus clustering (supplementary figure S2a), the consensus matrix (supplementary figure S2b) and the k-cluster distribution (supplementary figure S2c) showed $n=3$ as the optimal cluster number, supported by the cumulative distribution of the $k+1$ cluster (supplementary figure S2d). The RAC stability was good, as shown by the correct iterative classification (supplementary figure S2b). Clusters were clearly separated, with a slight overlap between RAC2 and RAC3 (supplementary figure S2e).

Quantitative HRCT

Supplementary table S8 shows values of all the radiological variables measured across asthma groups of different severity and healthy individuals. Table 2 shows representative qCT biomarkers across RACs and healthy control subjects. RAC2 patients had the highest qCT values reflecting airway wall thickness, including inspiratory WA average of mean values of right and left lung segmental bronchi (WA mean) ($p<0.01$ versus RAC1; $p<0.001$ versus RAC3) (supplementary table S7), and inspiratory ($p<0.0001$ versus either RAC1 or RAC3) (figure 1a and supplementary table S7) and expiratory WA standardised by body surface area (WA mean BSA) ($p<0.05$ versus RAC1; $p<0.0001$ versus RAC3) (table 2 and supplementary table S7). Compared with other RACs, RAC2 individuals also showed increased airway lumen area, including inspiratory ($p<0.001$ versus RAC1; $p<0.01$ versus RAC3) (table 2 and supplementary table S7) and expiratory LA average of median values of right and left lung segmental bronchi (LA median) ($p<0.01$ versus RAC1; $p<0.01$ versus RAC3) (figure 1b and supplementary table S7), and inspiratory ($p<0.0001$ versus RAC1; $p<0.05$ versus RAC3) (supplementary table S7) and expiratory LA average of mean values of right and left lung segmental bronchi standardised by BSA (LA mean BSA) ($p<0.01$ versus RAC1; $p<0.01$ versus RAC3) (supplementary table S7), all suggestive of predominant airway remodelling.

By contrast, RAC3 was characterised by predominant emphysematous-like changes as shown by the highest inspiratory LAA -950 HU ($p<0.0001$ versus RAC1; $p<0.001$ versus RAC2) (table 2 and figure 1c) and the lowest inspiratory percentile 15 ($p<0.0001$ versus RAC1; $p<0.01$ versus RAC2) (table 2 and figure 1d), and air trapping as reflected by the highest expiratory LAA -856 HU ($p<0.0001$ versus either RAC1 or RAC2) (table 2 and figure 1e). Inspiratory LAA -856 HU ($p<0.0001$ versus RAC1; $p<0.001$ versus RAC2) (supplementary table S7) and expiratory CT lung volume adjusted for the phantom density rods ($p<0.0001$ versus RAC1; $p<0.001$ versus RAC2) (figure 1f and supplementary table S7) were also elevated in RAC3, whereas lung density was reduced, as reflected by the lowest inspiratory ($p<0.0001$ versus RAC1; $p<0.05$ versus RAC2) (supplementary table S7) and expiratory MLD SD ($p<0.0001$ versus RAC1; $p<0.01$ versus RAC2) (supplementary table S7). All radiological values measured across all RACs are shown in supplementary table S7.

RAC1 individuals had no evidence of emphysematous-like changes or air trapping as reflected by inspiratory LAA -950 HU and expiratory LAA -856 HU values, respectively, similar to healthy individuals. In contrast, inspiratory adjusted CT lung volume ($p<0.0003$), reflecting lung volume, and inspiratory LA mean BSA ($p<0.0004$) and inspiratory LA median ($p<0.02$), reflecting lumen area, were reduced, while inspiratory ($p<0.0001$) and expiratory MLD SD ($p<0.02$), reflecting lung density, and Pct WA, reflecting airway wall thickness, were increased in RAC1 (supplementary table S9). Compared with healthy control subjects (supplementary tables S9–S11), airway wall thickness was increased in RAC2, as reflected by inspiratory WA mean ($p<0.04$) and inspiratory ($p<0.02$) and expiratory WA mean BSA ($p<0.004$) (supplementary table S10), but not in RAC1 (supplementary table S9) or RAC3 (supplementary table S11). In contrast, compared with healthy subjects, emphysematous-like changes, as reflected by inspiratory LAA -950 HU ($p<0.002$) and inspiratory percentile 15 ($p<0.0001$) were elevated in RAC3 (supplementary table S11), but not in RAC1 (supplementary table S9) or RAC2 (supplementary table S10). Compared with healthy control subjects, air trapping, as reflected by expiratory LAA -856 HU, was increased in RAC2 ($p<0.02$) (supplementary table S10) and, to a greater extent, in RAC3 ($p<0.0001$) (supplementary table S11). RAC1 showed reduced lung volume, as reflected by inspiratory adjusted CT lung volume ($p<0.0003$), and increased lung density, as reflected by inspiratory ($p<0.0001$) and expiratory MLD SD ($p<0.02$) (supplementary table S9). Based on asthma severity, there were no differences in qCT measurements except expiratory LAA -856 HU, elevated in severe asthma individuals, and inspiratory LA mean BSA, elevated in mild-to-moderate asthma individuals (supplementary table S8).

Clinical features of RAC phenotypes

No differences in scores for clinical questionnaires, including Asthma Control Questionnaire (ACQ)-5, Asthma Quality of Life Questionnaire, Hospital Anxiety and Depression Scale, and Sino-Nasal Outcomes Test-20, were observed across the RACs (table 1 and supplementary table S6). However, pairwise comparisons showed that mean ACQ-5 score was higher in RAC1 than in RAC2 ($p<0.02$) (table 1).

TABLE 2 Values of representative high-resolution computed tomography (CT) parameters used for clustering across radiomultiomic-associated clusters (RACs) and the healthy control subject (HS) group[#]

	RAC1		RAC2		RAC3		HS		p-value	RAC1 versus RAC2 p-value	RAC1 versus RAC3 p-value	RAC2 versus RAC3 p-value	RAC1 versus HS p-value	RAC2 versus HS p-value	RAC3 versus HS p-value	
	n	n	n	n	n	n										
Participants, n	30	34	41	15												
Inspiratory BSA (Mosteller formula)	2.12 (1.96–2.31)	30	1.98 (1.80–2.05)	34	1.94 (1.84–2.07)	41	2.01 (1.79–2.08)	15	0.0047	<0.01	<0.05	0.6547	0.0200	0.8427	0.9089	
Inspiratory adjusted CT lung volume, mm ³	4271 (3760–4842)	29	5553 (4990–6345)	34	6556 (5591–7448)	41	5239 (4613–6957)	15	<0.0001	<0.001	<0.0001	0.0028	<0.01	0.9464	0.0805	
Inspiratory LAA –950 HU, %	5.7 (3.6–9.5)	29	8.2 (6.0–10.4)	34	13.8 (10.3–17.9)	41	7.2 (3.8–12.8)	15	<0.0001	0.0384	<0.0001	<0.001	0.3500	0.6665	<0.01	
Inspiratory LA median, mm ²	16.7±0.8	29	21.7±0.8	30	18.0±0.7	41	20.1±1.4	14	0.0001	<0.001	0.1938	<0.01	<0.05	0.5161	0.0657	
Inspiratory percentile 15, HU	–914.9±4.4	29	–934.6±2.1	34	–947.8±1.8	41	–929.9±4.8	15	<0.0001	<0.0001	<0.0001	<0.01	<0.05	0.3050	<0.01	
Inspiratory WA mean BSA, mm ² ·m ^{–2}	14.1±0.4	29	18.9±0.5	30	15.7±0.4	41	16.6±0.8	14	<0.0001	<0.0001	0.2800	<0.0001	<0.05	<0.05	0.1642	
Expiratory LAA –856 HU, %	9.8±1.4	28	12.5±1.7	33	31.8±2.6	38	6.3±1.4	15	<0.0001	0.4137	<0.0001	<0.0001	0.1102	0.0268	<0.0001	
Expiratory WA mean BSA, mm ² ·m ^{–2}	13.9 (11.8–17.5)	18	18.6 (15.3–19.1)	27	12.9 (11.8–15.7)	34	14.0 (13.1–15.4)	14	<0.0001	<0.05	0.4615	<0.0001	0.6611	0.0032	0.1943	

Data for continuous variables are presented as mean±SEM or median (interquartile range). BSA: body surface area; adjusted CT lung volume: CT lung volume adjusted for the phantom density rods; LAA –950 HU: percentage of low attenuation area with CT number < –950 HU; LA median: lumen area average of median values of right and left lung segmental bronchi; percentile 15: 15th percentile of the cumulative frequency distribution of CT numbers; WA mean BSA: wall area average of mean values of right and left lung segmental bronchi standardised by BSA; LAA –856 HU: percentage of low attenuation area with CT number < –856 HU. [#]: only individuals with asthma were included in the cluster analysis (data from HS are shown as a control group). Normality of variables was tested using the D’Agostino and Pearson omnibus normality test. Between-group comparisons were performed using ANOVA with Tukey’s multiple comparison test for normally distributed data or the Kruskal–Wallis test with Dunn’s multiple comparison test for non-parametric data. Bold indicates significant p-values (p<0.05).

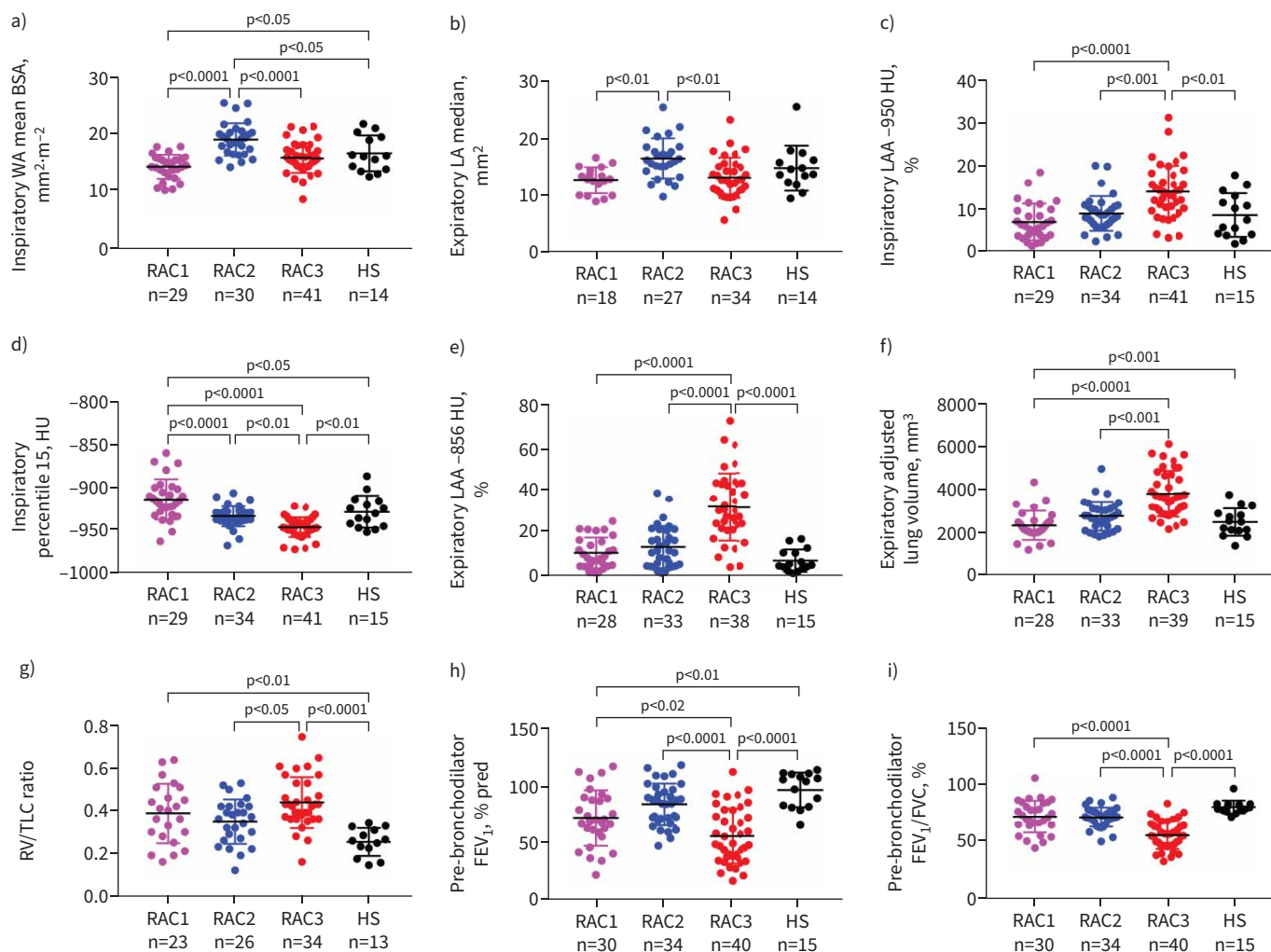


FIGURE 1 Scatter dot plots of selected quantitative computed tomography (qCT) parameters and pulmonary function tests across radiomultiomic-associated clusters (RACs) and healthy control subjects (HS). **a)** Inspiratory wall area average of mean values of right and left lung segmental bronchi standardised by body surface area (WA mean BSA). **b)** Expiratory lumen area average of median values of right and left lung segmental bronchi (LA median). **c)** Inspiratory percentage of low attenuation area with CT numbers < -950 HU (LAA -950 HU). **d)** Inspiratory 15th percentile of the cumulative frequency distribution of CT numbers (percentile 15). **e)** Expiratory percentage of low attenuation area with CT numbers < -856 HU (LAA -856 HU). **f)** Expiratory CT lung volume adjusted for the phantom density rods (adjusted CT lung volume). **g)** Residual volume/total lung capacity (RV/TLC) ratio. **h)** Pre-bronchodilator forced expiratory volume in 1 s (FEV_{1s}) percentage predicted. **i)** Pre-bronchodilator FEV_{1s} /forced vital capacity (FVC) ratio (percentage). Mean \pm SD or median with interquartile range values are shown depending on data distribution (see tables 1 and 2 and supplementary tables S6 and S7).

The percentage of mild-to-moderate asthma subjects within each RAC was similar (table 1). Demographic and clinical characteristics of individual RACs are shown in table 1. RAC1 was characterised by a higher prevalence of women (77%; RAC2=56%, RAC3=41%) (Chi-squared $p=0.013$) and obesity, as reflected by elevated body mass index (BMI) (36.8 ± 1.4 $\text{kg}\cdot\text{m}^{-2}$) compared with RAC2 ($p<0.0001$) and RAC3 ($p<0.0001$) (table 1), and elevated serum high-sensitivity C-reactive protein concentrations ($p=0.017$ versus RAC2; $p=0.002$ versus RAC3) and serum interleukin-6 ($p<0.003$ versus RAC2; $p<0.003$ versus RAC3) (supplementary table S6). Other clinical variables were similar across clusters (table 1 and supplementary table S6). Blood eosinophil counts, fractional exhaled nitric oxide (F_{ENO}) and serum total IgE concentrations, reflecting a type 2 (T2)-high phenotype, were similar across RACs. Except serum interleukin-6, variables reflecting a T2-low phenotype were similar across clusters (table 1 and supplementary table S6). However, pairwise comparisons showed that blood eosinophils were higher in RAC3 than in RAC1 ($p<0.04$) (table 1). The data suggest that airway remodelling mostly transcends the T2-high/low concept. Furthermore, all patients had some degree of reversibility, but this was significantly greater in patients in RAC3 compared to patients in RAC2 ($p=0.003$) (table 1). A Chi-squared analysis

($p=0.29$) suggests no strong association between smoking status and RACs in asthmatic subjects (supplementary table S12).

Pulmonary function tests

RAC3 showed the highest degree of airflow limitation, as reflected by elevated RV/TLC ratio ($p<0.05$ versus RAC2) (figure 1g), reduced pre-bronchodilator forced expiratory volume in 1 s (FEV_1) absolute ($p<0.001$ versus RAC2) (supplementary table S6) and percentage predicted values ($p<0.02$ versus RAC1; $p<0.0001$ versus RAC2) (table 1 and figure 1h), reduced pre-bronchodilator forced vital capacity (FVC) percentage predicted values ($p<0.001$ versus RAC2) (table 1), reduced FEV_1/FVC ($p<0.0001$ versus both RAC1 and RAC2) (table 1 and figure 1i), reduced pre-bronchodilator forced expiratory flow at 25–75% of FVC ($FEF_{25-75\%}$) absolute ($p<0.001$ versus RAC1; $p<0.001$ versus RAC2) (table 1) and percentage predicted values ($p<0.01$ versus RAC1; $p<0.0001$ versus RAC2) (table 1) and reduced pre-bronchodilator peak expiratory flow (PEF) percentage predicted values ($p<0.01$ versus RAC1; $p<0.0001$ versus RAC2) (table 1). RAC3 also showed reduced specific airway conductance compared with RAC2 ($p<0.002$) (table 1) and the highest degree of hyperinflation as reflected by RV ($p<0.0003$ versus RAC1; $p<0.0001$ versus RAC2) (table 1). Compared with healthy individuals, RV/TLC ratio was elevated in RAC1 ($p<0.01$) and RAC3 ($p<0.0001$) (figure 1g), but not in RAC2 participants, whereas FEV_1/FVC was reduced only in RAC3 participants ($p<0.0001$) (figure 1h). The bronchodilator reversibility test results showed greater increase in post-salbutamol FEV_1 percentage changes over baseline in RAC3 compared with RAC2 ($p<0.003$) (table 1).

qCT cluster replication

Based on 19 qCT biomarkers measured in both the discovery (supplementary table S7) and the matched ATLANTIS subset replication cohort (supplementary tables S13 and S14), three qCT clusters were identified in ATLANTIS (figure 2 and supplementary figure S3). Intra-cohort analysis, using our partial least square-linear discriminant analysis (PLS-LDA) classifier, indicated a strong performance within both the ATLANTIS and U-BIOPRED cohorts (table 3). In ATLANTIS, the classifier demonstrated a sensitivity of 0.88 (IQR 0.04), specificity of 0.94 (IQR 0.02), accuracy of 0.88 (IQR 0.05) and F1 score of 0.88 (IQR 0.04), while in U-BIOPRED, it achieved a sensitivity of 0.91 (IQR 0.08), specificity of 0.95 (IQR 0.03), accuracy of 0.91 (IQR 0.04) and F1 score of 0.90 (IQR 0.05). Moving to the inter-cohort analysis, where the classifier was tested across ATLANTIS–U-BIOPRED and U-BIOPRED–ATLANTIS cohorts, sensitivities ranged from 0.73 to 0.80, specificities from 0.85 to 0.89, accuracies from 0.72 to 0.79 and F1 scores from 0.73 to 0.78. In the combined analysis across both cohorts, the classifier achieved consistent performance with a sensitivity of 0.87 (IQR 0.06), specificity of 0.93 (IQR 0.02), accuracy of 0.88 (IQR 0.05) and F1 score of 0.87 (IQR 0.06) (table 3). These findings underscore the robustness and generalisability of our classifier across matched cohorts.

The trend of qCT biomarkers across qCT clusters in U-BIOPRED (table 2 and supplementary table S7) and ATLANTIS (supplementary table S13) was similar, although absolute values were lower in ATLANTIS (supplementary table S14). In both cohorts, inspiratory WA mean BSA, inspiratory and expiratory LA mean BSA and LA median were elevated in qCT cluster 2; and inspiratory LAA –950 HU and expiratory LAA –856 HU were elevated in qCT cluster 3 (tables 2 and supplementary tables S7 and S13). The clinical characteristics of both cohorts showed elevated BMI in qCT cluster 1 and reduced $FEV_1/FVC\%$, $FEF_{25-75\%}$ absolute and percentage predicted values, and specific airway conductance in qCT cluster 3 (table 1 and supplementary tables S6 and S15).

Molecular pathways of RACs

Molecular pathways identified by differentially expressed proteins and genes were selectively associated with individual RACs (figure 3, table 4, supplementary table S16 and supplementary figure S4). Most of the differences in pathways were observed between RAC2 and RAC3 and between RAC1 and RAC3 (figure 3). Serum and sputum proteomics could detect all differences in pathway modulation between RAC1 and RAC3, whereas endotype differences between RAC2 and RAC3 were dependent upon both transcriptomic and proteomic signals from multiple compartments (figure 3).

46 pathways were identified with adjusted $p<0.05$ (supplementary tables S3–S5). To visualise the pathway enrichment scores (table 4 and supplementary table S16) and molecular signatures across the RACs by omics datasets, we selected the serum proteomics dataset, because this is a readily accessible compartment and 25 over-represented pathways originated from this dataset (figure 4 and supplementary table S17). A heatmap shows correlations between CT parameters, lung function tests and enrichment scores of serum proteomics pathways (figure 5).

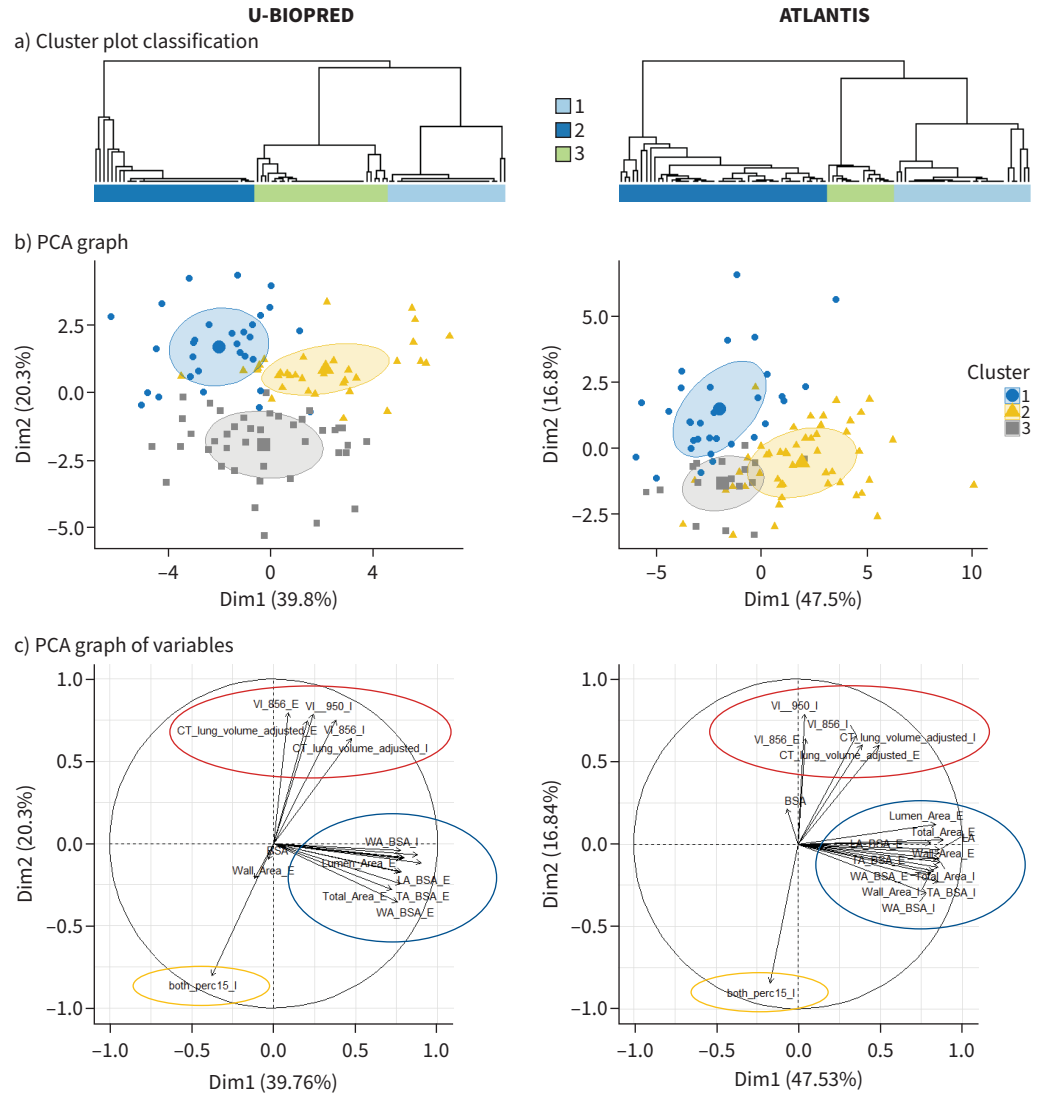


FIGURE 2 Comparative analysis of U-BIOPRED and ATLANTIS datasets across three analytical techniques. **a)** Clustering dendrograms of the consensus matrices for U-BIOPRED (left) and ATLANTIS (right) with the number of clusters $k=3$, illustrating the hierarchical clustering results and relationships between subjects based on their similarity. **b)** Principal component analysis (PCA) plots for U-BIOPRED (left) and ATLANTIS (right), where the first principal component (PC1) is plotted against the second principal component (PC2). Each dot represents a subject, coloured according to their membership in different quantitative computed tomography (qCT) clusters, highlighting the distribution and separation of subjects within the principal component space. **c)** Loadings of the used qCT features on PC1 and PC2 for U-BIOPRED (left) and ATLANTIS (right), showing the contribution and correlation of various qCT features to the principal components, aiding in understanding the underlying factors driving the clustering and separation observed in the subject-level PCA plots.

In bronchial biopsies, an extracellular matrix (ECM) organisation pathway, including fibulin-1 and latent transforming growth factor binding protein 2 (LTBP2) genes, functionally involved in tissue remodelling in respiratory diseases [23, 24], was upregulated in RAC2 compared with RAC1 ($p<0.02$) and RAC3 ($p<0.04$) (table 4, supplementary table S16 and supplementary figure S5a). RAC2 individuals also showed upregulation of the proliferative neurotrophic receptor tyrosine kinase 2/tyrosine kinase receptor B (NTRK2/TRKB) signalling, characterised by overexpression of the phosphatidylinositol-4,5-bisphosphate 3-kinase catalytic subunit α (PIK3CA) gene, using sputum transcriptomics, compared with RAC3 ($p<0.003$) (supplementary table S16 and supplementary figure S5b). Sputum proteomics also identified significant enrichment of ECM organisation (Kruskal–Wallis $p<0.04$) and interleukin molecular pathways (Kruskal–Wallis $p<0.02$), involving transforming growth factor (TGF)- β , in RAC2 individuals compared with RAC3 individuals (supplementary table S16 and supplementary figures S5c and d). In RAC2, sputum

TABLE 3 Performance metrics of prediction of quantitative computed tomography (qCT) clusters using a partial least squares linear discriminant analysis classifier on the CT measurements dataset from two cohorts, ATLANTIS and U-BIOPRED, for intra-cohort, inter-cohort and combined analyses

Cohort	Sensitivity	Specificity	Accuracy	F1 score
Intra-cohort				
ATLANTIS	0.88 (0.04)	0.94 (0.02)	0.88 (0.05)	0.88 (0.04)
U-BIOPRED	0.91 (0.08)	0.95 (0.03)	0.91 (0.04)	0.90 (0.05)
Inter-cohort				
ATLANTIS–U-BIOPRED	0.73	0.85	0.72	0.73
U-BIOPRED–ATLANTIS	0.80	0.89	0.79	0.78
Combined	0.87 (0.06)	0.93 (0.02)	0.88 (0.05)	0.87 (0.06)

Interquartile range is presented in brackets.

transcriptomics showed downregulation of the semaphorin interactions ($p < 0.04$ versus RAC1; $p < 0.004$ versus RAC3) and semaphorin 4D (SEMA4D) in semaphorin signalling ($p < 0.03$ versus RAC3) pathways (supplementary table S16)

In serum proteomics, the proliferative signalling by Erb-B2 receptor tyrosine kinase 2 (ERBB2) in cancer molecular pathway, characterised by elevated serum SHC adaptor protein 1 (SHC1), Erb-B4 receptor tyrosine kinase 4 (ERBB4), epidermal growth factor receptor (EGFR) and ERBB2, was upregulated in RAC2 ($p < 0.03$ versus RAC1; $p < 0.05$ versus RAC3) (table 4, supplementary table S16 and supplementary figure S5e). The semaphorin 3A (SEMA3A) p21-activated kinase (PAK)-dependent axon repulsion (table 4, supplementary table S16 and supplementary figure S5f) and semaphorin interactions pathways (supplementary table S16) were downregulated in RAC2 compared with RAC3 ($p < 0.0003$ for both). Cytokine signalling in the immune system (Kruskal–Wallis $p < 0.009$) (supplementary table S16 and supplementary figure S5g) and signalling by interleukin (Kruskal–Wallis $p < 0.004$) (table 4 and supplementary figure S5h) pathways, involving matrix metalloproteinase 1 (MMP1), MMP9 and nitric oxide synthase 2 (NOS2), and an ECM organisation pathway (Kruskal–Wallis $p < 0.04$) (supplementary table S16 and supplementary figure S5i), involving MMP2, were selectively elevated in RAC3 as shown by plasma proteomics and serum proteomics data, respectively.

RAC3 showed elevated signalling by NTRKs (Kruskal–Wallis $p < 0.002$) (table 4 and supplementary figure S6a), NTRK2/TRKB (Kruskal–Wallis $p < 0.002$) (table 4 and supplementary figure S6b), interleukins (Kruskal–Wallis $p < 0.05$) (supplementary table S16 and supplementary figure S6c) and intracellular second messengers (Kruskal–Wallis $p < 0.04$) (supplementary table S16 and supplementary figure S6d), as reflected by increased serum levels of various proteins, including protein tyrosine phosphatase non-receptor type 11 (PTPN11), also known as SH2 domain-containing protein tyrosine phosphatase 2 (SHP2) (table 4 and supplementary table S16).

In RAC1, proteomics showed upregulation of two complement cascade pathways in serum (Kruskal–Wallis $p < 0.00002$ and $p < 0.0002$) (table 4 and supplementary figure S6e and f), elevated activity of regulation of insulin-like growth factor (IGF) transport and uptake by IGF binding proteins (IGFBPs) pathway in serum (Kruskal–Wallis $p < 0.03$) (table 4 and supplementary figure S6g) and sputum (Kruskal–Wallis $p < 0.03$) (supplementary table S16 and supplementary figure S6h), and elevated signalling by leptin ($p < 0.05$) (supplementary table S3).

To summarise the results, we identified three qCT clusters in the severe asthma U-BIOPRED discovery cohort and replicated them in the matched ATLANTIS replication cohort. In the U-BIOPRED cohort, we found specific molecular pathways associated with individual qCT clusters, that we called RACs. However, we could not replicate these pathways because no asthma multiomic datasets with paired lung CT scan data are currently available.

Discussion

In this study, we performed an initial qCT-based clustering that identified three clusters in the U-BIOPRED cohort, which was replicated in the matched ATLANTIS cohort. We then proceeded to associate these qCT clusters with proteomics and transcriptomics data. We identified associations with specific pathways that have helped us to understand the potential pathogenetic mechanisms underlying airway wall remodelling and air trapping in severe asthma. To the best of our knowledge, this is the first attempt to apply the combination of qCT, transcriptomics, proteomics analyses and machine learning/AI.

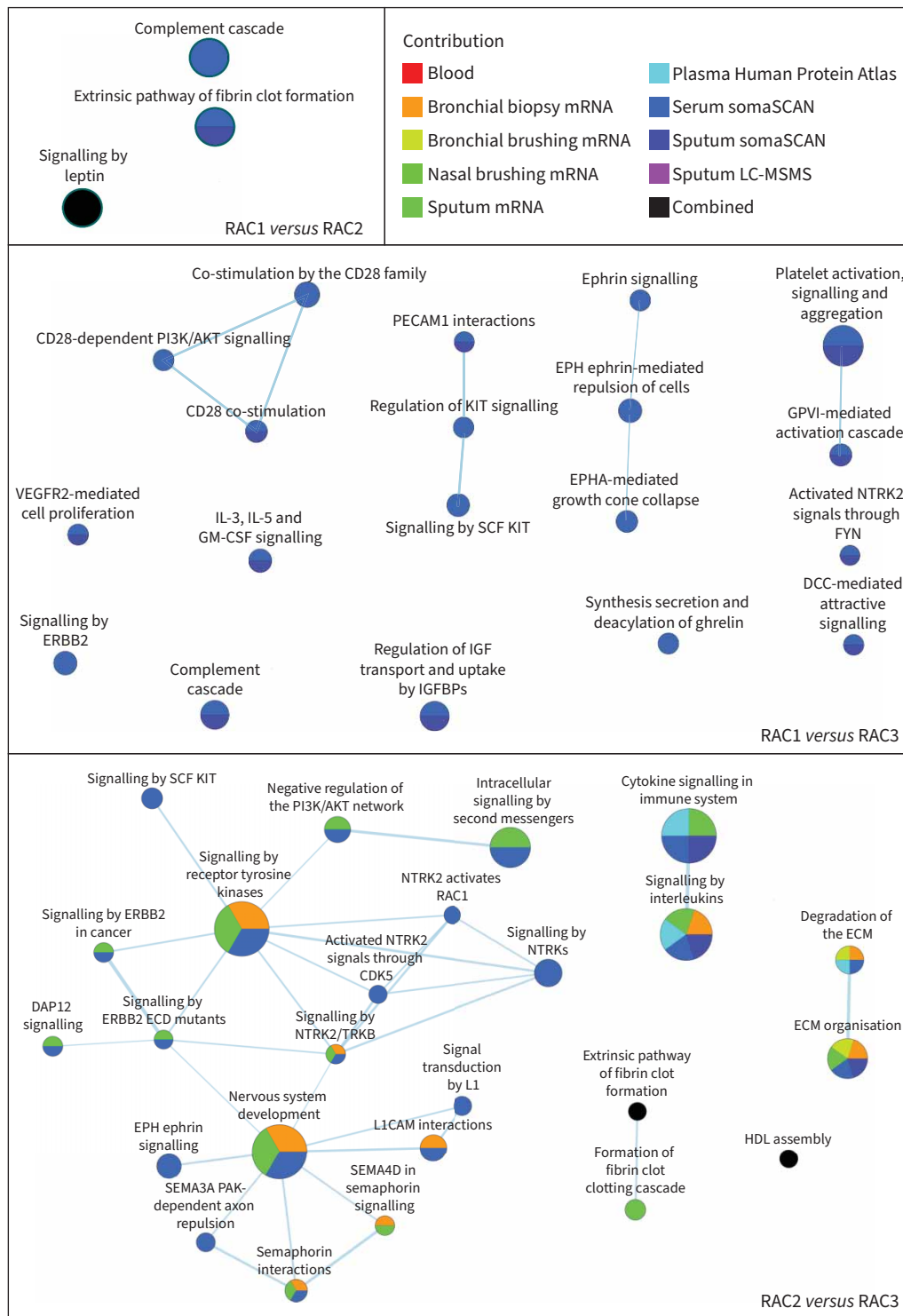


FIGURE 3 Enrichment maps for integrated pathway enrichment analysis in radiomultiomic-associated clusters (RACs). ActivePathways results are represented as enrichment maps, with nodes representing pathways and pathways with many shared genes connected into networks representing broader biological themes. Cytoscape software and the EnrichmentMap app were used to visualise integrated pathway enrichments as networks. Node colours correspond to the enriched pathways according to the supporting omics datasets, based on the scores matrix initially analysed in ActivePathways. See the supplementary material for a full list of definitions of abbreviations of genes, proteins and pathways.

TABLE 4 Overexpression of representative pathways/molecular phenotype expression across radiomultiomic-associated clusters (RACs)[#]

Pathway	Omic/biological matrix	RAC1 enrichment score	RAC2 enrichment score	RAC3 enrichment score	Kruskal–Wallis p-value	RAC1 versus RAC2 p-value	RAC1 versus RAC3 p-value	RAC2 versus RAC3 p-value	Overlapping genes or proteins
Complement cascade RAC1 versus RAC2	Proteomics/serum	0.54 (0.24–0.67)	−0.05 (−0.35–0.23)	0.07 (−0.33–0.37)	1.3e-05	1e-05	2e-05	0.598561	CFH, CFI, C5, C9, C1S, CFD
Complement cascade RAC1 versus RAC3	Proteomics/serum	0.48 (0.21–0.64)	0.09 (−0.19–0.35)	−0.08 (−0.36–0.32)	0.00015	0.00113	5e-05	0.27836	CFI, C9, CFH, C5, CD55, C3, FCN1, CRP
Signalling by ERBB2 in cancer	Proteomics/serum	−0.16 (−0.32–0.07)	0.08 (−0.14–0.26)	−0.09 (−0.29–0.17)	0.05125	0.02194	0.74612	0.049392	SHC1, ERBB4, EGFR, ERBB2
ECM organisation	Transcriptomics/bronchial biopsy	−0.31 (−0.36–0.15)	0.21 (−0.10–0.38)	−0.42 (−0.48–0.03)	0.0184	0.01592	0.28238	0.03649	DCN, ITGA6, LAMA4, DDR2, FBLN1, CTSB, LTBP2, DST, LTBP4
GPVI-mediated activation cascade	Proteomics/serum	−0.56 (−0.72–0.10)	−0.35 (−0.66–0.03)	0.27 (−0.49–0.59)	0.00146	0.283067	0.001364	0.00539	PTPN6, LYN, FYN, PDPK1, CLEC1B, GP6
Regulation of KIT signalling	Proteomics/serum	−0.53 (−0.78–0.03)	−0.33 (−0.58–0.09)	0.26 (−0.38–0.64)	0.00494	0.12495	0.00268	0.04282	PTPN6, LYN, FYN, SRC
Regulation of IGF transport and uptake by IGFs	Proteomics/serum	0.43 (0.35–0.52)	−0.15 (−0.26–0.03)	−0.20 (−0.44–0.07)	0.02478	0.13333	0.00586	0.92308	C3, MFG8, FN1, PAPP, ALB, GPC3, SPARCL1, F2, FGG, MEP
Degradation of the ECM	Proteomics/serum	−0.17 (−0.31–0.05)	−0.02 (−0.20–0.13)	0.08 (−0.19–0.30)	0.01557	0.10863	0.00596	0.13233	COL23A1, MMP2, BSG, CASP3, MMP12, KLK7, MMP17, ADAMTS5
Signalling by interleukins	Proteomics/plasma	−0.25 (−0.46–0.22)	−0.22 (−0.33–0.06)	0.14 (−0.16–0.41)	0.0038	0.88862	0.00886	0.00183	TSLP, NFKB2, NOS2, MMP9, MMP1, CCL11, IFNG, HSP90B1, ANXA2
Signalling by SCF KIT	Proteomics/serum	−0.41 (−0.56–0.02)	−0.26 (−0.45–0.08)	0.07 (−0.33–0.50)	0.00968	0.35257	0.00620	0.02438	RAC1, PTPN11, TEC, PTPN6, FER, LYN, PRKCA, SRC, JAK2, LCK
Signalling by NTRKs	Proteomics/serum	−0.32 (−0.42–0.24)	−0.36 (−0.52–0.12)	0.09 (−0.20–0.41)	0.00109	0.26896	0.03042	0.00019	RAC1, SHC1, PTPN11, RPS6KA3, ADCYAP1, CRK, MAPK1, DUSP3
DAP1 signalling	Proteomics/serum	−0.34 (−0.65–0.18)	−0.47 (−0.68–0.22)	0.28 (−0.39–0.60)	0.00131	0.35257	0.01193	0.00053	RAC1, SHC1, BTK
SEMA3A PAK-dependent axon repulsion	Proteomics/serum	−0.28 (−0.65–0.17)	−0.54 (−0.67–0.20)	0.27 (−0.22–0.53)	0.00084	0.24218	0.01539	0.00026	CFL1, RAC1
Signalling by NTRK2/TRKB	Proteomics/serum	−0.21 (−0.62–0.15)	−0.47 (−0.68–0.29)	0.17 (−0.13–0.61)	0.00106	0.11975	0.03245	3e-04	RAC1, SHC1, PTPN11

Enrichment scores are presented as median (interquartile range). #: the complete list of enrichment of molecular pathways across RACs is shown in supplementary table S16. See the supplementary material for a full list of definitions of abbreviations of genes, proteins and pathways. Datasets: Bronchial biopsy transcriptomics: RAC1, n=8; RAC2, n=13; RAC3, n=6. Sputum transcriptomics: RAC1, n=3; RAC2, n=5; RAC3, n=14. Plasma proteomics: RAC1, n=29; RAC2, n=33; RAC3, n=36. Serum proteomics: RAC1, n=27; RAC2, n=30; RAC3, n=41. Sputum proteomics: RAC1, n=4; RAC2, n=2; RAC3, n=11. Between-group comparisons were performed using the Kruskal–Wallis test with Dunn’s multiple comparison test. Bold indicates significant p-values (p<0.05).

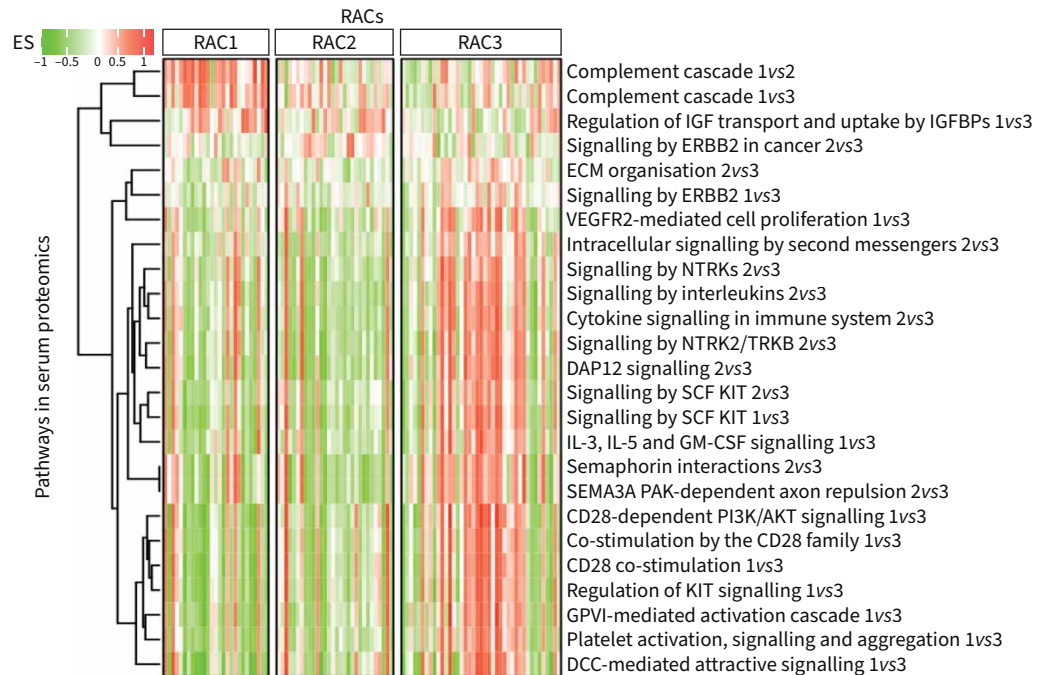


FIGURE 4 Modulation of serum proteomic pathways in severe asthma radiomultiomic-associated clusters (RACs). Enrichment scores (ESs) of 25 pathways (rows) are illustrated for subjects (columns) segmented by RACs. For each column, pathway names are shown on the right. Signatures and a list of proteins that represent a subset of pathways are shown in supplementary table S17. Serum proteins are measured by the somasCAN proteomics and are differentially expressed across RACs (shown at the end of the pathway names for each comparison, e.g. 1vs2). See the supplementary material for a full list of definitions of abbreviations of genes, proteins and pathways.

The three RACs were defined by differences in airway wall thickness and size, the degree of air trapping, and changes in lung density. RAC1 showed airway wall dimensions similar to healthy controls, but with reduced areas of low density and lower lung volumes. Compared with healthy subjects, RAC2 was characterised by increased airway wall thickness and mild air trapping, which was more pronounced in RAC3; only RAC3 showed the presence of large lungs and increasing lung areas of low density. The lung function indices showed that RAC1 had mild airflow obstruction, RAC2 mild reduction in peripheral airways function, and RAC3 the most severe degree of airflow obstruction and increased TLC and RV consistent with qCT biomarkers of air trapping changes that could underlie the severe airflow obstruction. Finally, RAC1 individuals were the most obese group.

We have externally replicated U-BIOPRED qCT clusters in a matched independent asthmatic cohort with a cross-replication balanced accuracy >0.80. Although qCT biomarker values in ATLANTIS were generally lower than those in U-BIOPRED, the trend across qCT clusters within each cohort was similar, with measures reflecting airway wall thickness and LA elevated in both qCT clusters 2 and those reflecting LAAs and air trapping elevated in both qCT clusters 3.

Compared with RAC3, RAC2 showed upregulation of an ECM organisation molecular pathway in bronchial biopsy involving fibulin-1 and LTBP2 genes, which contribute to airway remodelling [23, 24]. Fibulin-1 binding to LTBP2 activates TGF- β /Smad2 signalling [23, 24], a pivotal mechanism in airway remodelling [25]. RAC2 also showed upregulation of proliferative pathways, including signalling by NTRK2/TRKB, characterised by overexpression of the PIK3CA gene, and signalling by ERBB2 in cancer, as reflected by elevated serum concentrations of SHC1, ERBB4, EGFR and ERBB2, compared with RAC3. PIK3CA plays a pivotal role in human airway smooth muscle (ASM) cell proliferation [26, 27]. Our findings support a role for enhanced EGFR signalling in asthma airway remodelling [28, 29] and might suggest a functional involvement of ERBB2, also known as human epidermal growth factor receptor 2 (HER2), and ERBB4, also known as HER4, in its pathogenesis [30].



FIGURE 5 Heatmap showing the correlations between serum proteomics pathways and lung function (LF) tests and quantitative computed tomography (qCT) parameters in the three radiomultiomic-associated clusters (RACs). Positive correlations are shown in red; negative correlations are shown in green. See the supplementary material for a full list of definitions of abbreviations of genes, proteins and pathways. See the main text and supplementary table S2 for the definitions and details of the qCT parameters.

In contrast, serum proteomics indicated downregulation of the SEMA3A PAK-dependent axon repulsion pathway in RAC2. Likewise, sputum transcriptomics showed downregulation of the semaphorin interactions and SEMA4D in semaphorin signalling pathways. The data support the anti-remodelling effects of semaphorins reported in human ASM cells from asthma individuals *in vitro* [31] and in an *in vivo* mouse model of allergic asthma [32].

Serum proteomics in RAC3 showed upregulation of molecular pathways involving PTPN11, including cytokine signalling in the immune system, signalling by stem cell factor (SCF) KIT and signalling by NTRKs. PTPN11 has been shown to upregulate cigarette smoke-induced epithelial–mesenchymal transition by increasing MMP9 production in mouse lungs *in vivo* and in pulmonary epithelial cell cultures *in vitro* [33]. Serum proteomics also showed upregulation of cytokine signalling in the immune system and signalling by interleukin pathways involving MMP1, MMP9 and NOS2 in RAC3. These findings are consistent with elevated serum concentrations of MMPs in COPD individuals with emphysema [34] and with a role for NOS2 in mediating emphysematous remodelling [35].

The data highlight the importance of the pathways dysregulation, as subtle differences in pathway activation or molecular components may alter the overall functionality. As an example, the ECM organisation pathway characterised by elevated fibulin-1 and LTBP2 gene expression in bronchial biopsies was upregulated in RAC2, whereas the ECM organisation pathway, including collagen type XXIII α 1 chain, collagen type IX α 2 chain, syndecan 1 and tenascin C gene expression in sputum cells, was downregulated in RAC2. These data suggest different pathogenetic mechanisms underlying remodelling in the peripheral airways (RAC2) and in the lungs (RAC3). However, opposite regulation of individual pathways/molecular phenotypes in the same RAC might also be explained by different omics (transcriptomics, proteomics) and biological matrices used for analyses. The lack of correlation of the airway remodelling pathways with FEV₁ can only be explained by an effect on ASM mass or on subepithelial fibrosis. We cannot check this but we would assume that there was a greater effect on subepithelial fibrosis rather than on ASM mass. The relationships between the modulation of selected ECM organisation pathways, inflammation and remodelling in RAC2 and RAC3 have to be clarified.

RAC1 was characterised by the presence of obesity, and upregulation of the complement pathway and leptin signalling. These findings are consistent with a 7-year longitudinal cohort study which has shown that activation of the complement system could be involved in the development of obesity [36]. Alternatively, the activation of the complement cascade might be a consequence of obesity [37].

The number of omics required to obtain the most complete information on molecular phenotype differences across RACs depends on the RAC pair comparisons. This supports the utility of radiomultiomics in deeply characterising severe asthma molecular endotypes. By combining structural and molecular information, radiomultiomics might provide a unique tool to explore the pathophysiological heterogeneity of severe asthma with the ultimate goal of predicting individual disease trajectories and therapeutic response.

Our study underscores the significance of inter-cohort generalisation and the advantages of combining datasets. Although CT measurements exhibited robust predictive capabilities within the distinct ATLANTIS and U-BIOPRED cohorts, cross-cohort assessments unveiled a marginal decline in performance. Nevertheless, through dataset amalgamation, we attained heightened predictive accuracy. This highlights the pivotal role of expansive and diverse datasets in refining predictive models for respiratory health outcomes. However, our study has some limitations, including the inability to determine a causative link between modulation of molecular phenotypes and airway remodelling and/or emphysematous-like changes, which requires future mechanistic studies and the use of one-sided rather than two-sided procedures for pooling p-values. In our study, the distribution of smokers/ex-smokers across RACs and their smoking exposure assessed by pack-years was similar, which would exclude a prominent role of smoking. However, further research is required to establish the potential effects of smoking on molecular pathways associated with RACs. HRCT longitudinal studies are required to determine the behaviour of RACs over time, their response to endotype-based pharmacotherapies, including anti-T2 therapies, and the effect of environmental exposure. The number of individuals with transcriptomic and proteomic data from all compartments studied (sputum, biopsies and blood) was also limited. These transcriptomic and proteomic molecular phenotypes characterising individual RACs require external replication in independent datasets from other severe asthma cohorts that have these corresponding parameters, but these do not currently exist.

In conclusion, we showed that qCT clusters can be replicated in an external matched severe asthma cohort and that they are associated with the modulation of specific molecular pathways. Including multiomics data

and machine learning/AI into CT scan assessment might expand its diagnostic potential, while integrating CT scan data into multiomic studies might provide molecular pathway analysis with non-invasive structural correlates. This approach is of potential general application. By providing unique insights into the possible pathogenetic mechanisms associated with severe asthma heterogeneity, radiomultiomics might pave the way for a new approach to personalised medicine.

Acknowledgements: To my Beloved Mamma Laura, always with me, Paolino.

Some of this work has been presented previously in abstract form (<https://doi.org/10.1183/13993003.congress-2022.1214>).

Ethics statement: The U-BIOPRED study was approved by the ethics committee at each recruiting centre. Written informed consent was obtained from all participants.

Conflict of interest: K.F. Chung reports grants from the MRC, EPSRC, GSK, Merck and NIEHS, payment or honoraria for lectures, presentations, manuscript writing or educational events from GSK, Novartis and AstraZeneca, and participation on a data safety monitoring board or advisory board with GSK, AstraZeneca, Novartis, Roche, Merck, Trevi, Rickett-Beckinson, Nocion, Shionogi and Clean Breathing Institute supported by Haleon. C. Auffray reports support for the present study from the Innovative Medicines Initiative. Y. Badi reports support for the present study from the Innovative Medicines Initiative. P. Bakke reports payment or honoraria for lectures, presentations, manuscript writing or educational events from AstraZeneca, GSK and Sanofi. C. Brightling reports support for the present study from the ATLANTIS study (Chiesi grant) and Leicester NIHR BRC, grants from 4D Pharma, Areteia, AstraZeneca, Chiesi, Genentech, GSK, Mologic, Novartis, Regeneron Pharmaceuticals, Roche and Sanofi, and consultancy fees from 4D Pharma, Areteia, AstraZeneca, Chiesi, Genentech, GSK, Mologic, Novartis, Regeneron Pharmaceuticals, Roche and Sanofi. P. Chaney reports grants from ALK, AstraZeneca, Boehringer Ingelheim, Chiesi, GSK, Menarini, Novartis and Sanofi Aventis, consultancy fees from ALK, AstraZeneca, Boehringer Ingelheim, Chiesi, GSK, Menarini, Novartis and Sanofi Aventis, payment or honoraria for lectures, presentations, manuscript writing or educational events from ALK, AstraZeneca, Boehringer Ingelheim, Chiesi, GSK, Menarini, Novartis and Sanofi Aventis, and support for attending meetings from ALK, AstraZeneca, Boehringer Ingelheim, Chiesi, GSK, Menarini, Novartis and Sanofi Aventis. B. De Meulder reports support for the present study from the Innovative Medicines Initiative. R. Djukanovic reports consultancy fees from Synairgen plc, GSK, ZenasBio and Celltrion, leadership role as Chair of the European Respiratory Society's clinical research collaboration on severe asthma (SHARP), and stock (or stock options) with Synairgen plc. L. Fabbri reports consultancy fees from Chiesi Farmaceutici and AstraZeneca, payment or honoraria for lectures, presentations, manuscript writing or educational events from Chiesi Farmaceutici, AstraZeneca, GSK, Alfasigma and Novartis, support for attending meetings from Chiesi Farmaceutici, GSK and Novartis, and participation on a data safety monitoring board or advisory board with Novartis and Chiesi. S.J. Fowler reports grants from the NIHR, and payment or honoraria for lectures, presentations, manuscript writing or educational events from Boehringer Ingelheim. P. Howarth reports employment with GSK. J. Kolmert reports consultancy fees from Gesynta Pharma AB and Lipum AB. M. Kraft reports grants from the NIH, American Lung Association, Synairgen, Janssen, AstraZeneca and Sanofi, consultancy fees from AstraZeneca, Sanofi, Chiesi, GSK, Kinaset and Genentech, payment or honoraria for lectures, presentations, manuscript writing or educational events from Chiesi, support for attending meetings from the European Respiratory Society, one patent issued and tiled filed to development of therapeutics for inflammatory lung disease as CoFounder and Chief Medical Officer, RaeSedo, Inc., participation on a data safety monitoring board or advisory board with ALung, leadership role with the National Heart, Lung and Blood Advisory Council, stock (or stock options) with RaeSedo, Inc. (equity ownership), and the following financial (or non-financial) interests: Section Editor of UpToDate. A.H. Maitland-van der Zee reports grants from Health Holland, GSK, Boehringer Ingelheim and Vertex, consultancy fees from Boehringer Ingelheim and AstraZeneca, payment or honoraria for lectures, presentations, manuscript writing or educational events from GSK, and participation on a data safety monitoring board or advisory board for a study on BPD in neonates. A. Papi reports grants from Chiesi, AstraZeneca, GSK and Sanofi, consultancy fees from Chiesi, AstraZeneca, GSK, Novartis, Sanofi, Iqvia, Avillion, Elpen Pharmaceuticals, Moderna and Roche, payment or honoraria for lectures, presentations, manuscript writing or educational events from Chiesi, AstraZeneca, GSK, Menarini, Zambon, Mundipharma, Sanofi, Edmond Pharma, Iqvia, Avillion, Sanofi and Regeneron, participation on a data safety monitoring board or advisory board with Chiesi, AstraZeneca, GSK, Novartis, Sanofi, Iqvia, Avillion, Elpen Pharmaceuticals and Moderna, receipt of equipment, materials, drugs, medical writing, gifts or other services from Consorzio Futuro in Ricerca. K. Rabe reports payment or honoraria for lectures, presentations, manuscript writing or educational events from AstraZeneca, Boehringer Ingelheim, Chiesi Pharmaceuticals, Novartis, Sanofi/Regeneron, GSK, Berlin Chemie and Roche Pharma, participation on a data safety monitoring board or advisory board with AstraZeneca, Boehringer Ingelheim, Sanofi/Regeneron and CSL Behring, and leadership roles with the German Center for Lung Research (DZL), German Chest Society (DGP) and American

Thoracic Society. D.E. Shaw reports consultancy fees from GSK, AstraZeneca and Novartis, payment or honoraria for lectures, presentations, manuscript writing or educational events from GSK and AstraZeneca, and support for attending meetings from GSK. D. Singh reports consultancy fees from Aerogen, AstraZeneca, Boehringer Ingelheim, Chiesi, Cipla, CSL Behring, EpiEndo, Genentech, GSK, Glenmark, Gossamer Bio, Kinaset Therapeutics, Menarini, Novartis, Orion, Pulmatrix, Sanofi, Synairgen, Teva, Theravance, Biopharma and Verona Pharma. M. van Den Berge reports grants from GSK, Roche, Genentech and Novartis. Y. Guo reports support for the present study from the Innovative Medicines Initiative. S. Wagers reports consultancy fees from King's College Hospital NHS Foundation Trust, Academic Medical Research, AMC Medical Research BV, Asthma UK, Athens Medical School, Boehringer Ingelheim International GmbH, CHU de Toulouse, CIRO, DS Biologicals Ltd, École Polytechnique Fédérale De Lausanne, European Respiratory Society, FISEVI, Fluidic Analytics Ltd, Fraunhofer IGB, Fraunhofer ITEM, GSK Research & Development Ltd, Holland & Knight, Karolinska Institutet Fakturor, KU Leuven, Longfonds, National Heart and Lung Institute, Novartis Pharma AG, Owlstone Medical Limited, PEXA AB, UCB Biopharma SPRL, Umeå University, University Hospital Southampton NHS Foundation Trust, Università Campus Bio-Medico di Roma, Università Cattolica Del Sacro Cuore, Universität Ulm, University of Bern, University of Edinburgh, University of Hull, University of Leicester, University of Loughborough, University of Luxembourg, University of Manchester, University of Nottingham, Vlaams Brabant, Dienst Europa, Imperial College London, Boehringer Ingelheim, Breathomix, Gossamer Bio, AstraZeneca, CIBER, OncoRadiomics, University of Leiden, University of Wurzburg, Chiesi Pharmaceutical, University of Liege, Teva Pharmaceuticals, Sanofi, Pulmonary Fibrosis Foundation and Three Lakes Foundation. P.J. Sterk reports consultancy fees from SME Breathomix, and stock (or stock options) with SME Breathomix. S-E. Dahlen reports grants from AstraZeneca, GSK and Sanofi, consultancy fees from AstraZeneca, Cayman Chemicals, GSK and Regeneron, and payment or honoraria for lectures, presentations, manuscript writing or educational events from AstraZeneca, GSK and Sanofi. I.M. Adcock reports support for the present study from the Innovative Medicines Initiative, grants from GSK, MRC, EPSRC and Sanofi, consultancy fees from GSK, Sanofi, Chiesi and Kinaset, payment or honoraria for lectures, presentations, manuscript writing or educational events from AstraZeneca, Sanofi, Eurodrug and Sunovion, and support for attending meetings from AstraZeneca. S. Siddiqui consultancy fees from AstraZeneca, GSK, CSL Behring, Areteia Therapeutics, ERT Medical, Chiesi and Roche, and payment or honoraria for lectures, presentations, manuscript writing or educational events from GSK, Chiesi and AstraZeneca. P. Montuschi reports support for the present study from the Innovative Medicines Initiative. The remaining authors have no potential conflicts of interest to disclose.

Support statement: U-BIOPRED is supported through an Innovative Medicines Initiative Joint Undertaking under grant agreement number 115010, resources of which are composed of financial contributions from the European Union's Seventh Framework Programme (FP7/2007–2013) and EFPIA companies' in-kind contribution (www.imi.europa.eu). Funding information for this article has been deposited with the Crossref Funder Registry.

References

- 1 Aysola RS, Hoffman EA, Gierada D, *et al.* Airway remodeling measured by multidetector CT is increased in severe asthma and correlates with pathology. *Chest* 2008; 134: 1183–1191.
- 2 Gupta S, Siddiqui S, Haldar P, *et al.* Quantitative analysis of high-resolution computed tomography scans in severe asthma subphenotypes. *Thorax* 2010; 65: 775–781.
- 3 Brillet PY, Grenier PA, Fetita CI, *et al.* Relationship between the airway wall area and asthma control score in moderate persistent asthma. *Eur Radiol* 2013; 23: 1594–1602.
- 4 Niimi A, Matsumoto H, Amitani R, *et al.* Airway wall thickness in asthma assessed by computed tomography. Relation to clinical indices. *Am J Respir Crit Care Med* 2000; 162: 1518–1523.
- 5 Chetta A, Foresi A, Del Donno M, *et al.* Airways remodeling is a distinctive feature of asthma and is related to severity of disease. *Chest* 1997; 111: 852–857.
- 6 Busacker A, Newell JD Jr, Keefe T, *et al.* A multivariate analysis of risk factors for the air-trapping asthmatic phenotype as measured by quantitative CT analysis. *Chest* 2009; 135: 48–56.
- 7 Trivedi AP, Hall C, Goss CW, *et al.* Quantitative CT characteristics of cluster phenotypes in the Severe Asthma Research Program cohorts. *Radiology* 2022; 304: 450–459.
- 8 Gupta S, Hartley R, Khan UT, *et al.* Quantitative computed tomography-derived clusters: redefining airway remodeling in asthmatic patients. *J Allergy Clin Immunol* 2014; 133: 729–773.
- 9 Zhang X, Xia T, Lai Z, *et al.* Uncontrolled asthma phenotypes defined from parameters using quantitative CT analysis. *Eur Radiol* 2019; 29: 2848–2858.
- 10 Choi S, Hoffman EA, Wenzel SE, *et al.* Quantitative computed tomographic imaging-based clustering differentiates asthmatic subgroups with distinctive clinical phenotypes. *J Allergy Clin Immunol* 2017; 140: 690–700.
- 11 Shaw DE, Sousa AR, Fowler SJ, *et al.* Clinical and inflammatory characteristics of the European U-BIOPRED adult severe asthma cohort. *Eur Respir J* 2015; 46: 1308–1321.

- 12 Kraft M, Richardson M, Hallmark B, *et al.* The role of small airway dysfunction in asthma control and exacerbations: a longitudinal, observational analysis using data from the ATLANTIS study. *Lancet Respir Med* 2022; 10: 661–668.
- 13 Chung KF, Wenzel SE, Brozek JL, *et al.* International ERS/ATS guidelines on definition, evaluation and treatment of severe asthma. *Eur Respir J* 2014; 43: 343–373.
- 14 De Meulder B, Lefaudeux D, Bansal AT, *et al.* A computational framework for complex disease stratification from multiple large-scale datasets. *BMC Syst Biol* 2018; 12: 60.
- 15 Wilson SJ, Ward JA, Pickett HM, *et al.* Airway elastin is increased in severe asthma and relates to proximal wall area: histological and computed tomography findings from the U-BIOPRED severe asthma study. *Clin Exp Allergy* 2021; 51: 296–304.
- 16 Ho DE, Kosuke I, King G, *et al.* Matching as nonparametric preprocessing for reducing model dependence in parametric causal inference. *Polit Anal* 2007; 15: 199–236.
- 17 Shannon P, Markiel A, Ozier O, *et al.* Cytoscape: a software environment for integrated models of biomolecular interaction networks. *Genome Res* 2003; 13: 2498–2504.
- 18 Wilkerson MD, Hayes DN. ConsensusClusterPlus: a class discovery tool with confidence assessments and item tracking. *Bioinformatics* 2010; 26: 1572–1573.
- 19 Paczkowska M, Barenboim J, Sintupisut N, *et al.* Integrative pathway enrichment analysis of multivariate omics data. *Nat Commun* 2020; 11: 735.
- 20 Brown MB. 400: A method for combining non-independent, one-sided tests of significance. *Biometrics* 1975; 31: 987–992.
- 21 Fabregat A, Sidiropoulos K, Viteri G, *et al.* Reactome diagram viewer: data structures and strategies to boost performance. *Bioinformatics* 2018; 34: 1208–1214.
- 22 Hänzelmann S, Castelo R, Guinney J. GSEA: gene set variation analysis for microarray and RNA-seq data. *BMC Bioinformatics* 2013; 14: 7.
- 23 Liu G, Cooley MA, Jarnicki AG, *et al.* Fibulin-1 regulates the pathogenesis of tissue remodeling in respiratory diseases. *JCI Insight* 2016; 1: e86380.
- 24 Liu G, Cooley MA, Jarnicki AG, *et al.* Fibulin-1c regulates transforming growth factor- β activation in pulmonary tissue fibrosis. *JCI Insight* 2019; 5: e124529.
- 25 Sagara H, Okada T, Okumura K, *et al.* Activation of TGF-beta/Smad2 signaling is associated with airway remodeling in asthma. *J Allergy Clin Immunol* 2002; 110: 249–254.
- 26 Krymskaya VP, Ammit AJ, Hoffman RK, *et al.* Activation of class IA PI3K stimulates DNA synthesis in human airway smooth muscle cells. *Am J Physiol Lung Cell Mol Physiol* 2001; 280: L1009–L1018.
- 27 Hu R, Pan W, Fedulov AV, *et al.* MicroRNA-10a controls airway smooth muscle cell proliferation via direct targeting of the PI3 kinase pathway. *FASEB J* 2014; 28: 2347–2357.
- 28 Puddicombe SM, Polosa R, Richter A, *et al.* Involvement of the epidermal growth factor receptor in epithelial repair in asthma. *FASEB J* 2000; 14: 1362–1374.
- 29 Homma T, Kato A, Sakashita M, *et al.* Involvement of Toll-like receptor 2 and epidermal growth factor receptor signaling in epithelial expression of airway remodeling factors. *Am J Respir Cell Mol Biol* 2015; 52: 471–481.
- 30 Inoue H, Akimoto K, Homma T, *et al.* Airway epithelial dysfunction in asthma: relevant to epidermal growth factor receptors and airway epithelial cells. *J Clin Med* 2020; 9: 3698.
- 31 Movassagh H, Tatari N, Shan L, *et al.* Human airway smooth muscle cell proliferation from asthmatics is negatively regulated by semaphorin3A. *Oncotarget* 2016; 7: 80238–80251.
- 32 Movassagh H, Shan L, Mohammed A, *et al.* Semaphorin 3E deficiency exacerbates airway inflammation, hyperresponsiveness, and remodeling in a mouse model of allergic asthma. *J Immunol* 2017; 198: 1805–1814.
- 33 Liu YN, Guan Y, Shen J, *et al.* Shp2 positively regulates cigarette smoke-induced epithelial mesenchymal transition by mediating MMP-9 production. *Respir Res* 2020; 21: 161.
- 34 Navratilova Z, Zatloukal J, Kriegova E, *et al.* Simultaneous up-regulation of matrix metalloproteinases 1, 2, 3, 7, 8, 9 and tissue inhibitors of metalloproteinases 1, 4 in serum of patients with chronic obstructive pulmonary disease. *Respirology* 2012; 17: 1006–1012.
- 35 Knudsen L, Atochina-Vasserman EN, Massa CB, *et al.* The role of inducible nitric oxide synthase for interstitial remodeling of alveolar septa in surfactant protein D-deficient mice. *Am J Physiol Lung Cell Mol Physiol* 2015; 309: L959–L969.
- 36 Xin Y, Hertle E, van der Kallen CJH, *et al.* Longitudinal associations of the alternative and terminal pathways of complement activation with adiposity: the CODAM study. *Obes Res Clin Pract* 2018; 12: 286–292.
- 37 Pinkerton JW, Kim RY, Brown AC, *et al.* Relationship between type 2 cytokine and inflammasome responses in obesity-associated asthma. *J Allergy Clin Immunol* 2022; 149: 1270–1280.